

# Dynamical heterogeneities approaching the binary colloidal glass transition

Takayuki Narumi,<sup>1,\*</sup> Scott V. Franklin,<sup>2</sup> Michio Tokuyama,<sup>3,4</sup> and Eric R. Weeks<sup>5</sup>

<sup>1</sup>*Department of Nanomechanics, Tohoku University, Sendai, Japan 980-8579*

<sup>2</sup>*Department of Physics, Rochester Institute of Technology, Rochester, NY 14623-5603*

<sup>3</sup>*WPI Advanced Institute for Material Research, Tohoku University, Sendai, Japan 980-8577*

<sup>4</sup>*Institute of Fluid Science, Tohoku University, Sendai, Japan 980-8577*

<sup>5</sup>*Physics Department, Emory University, Atlanta, Georgia 30322*

(Dated: November 3, 2009)

We study concentrated binary colloidal suspensions, a model system which has a glass transition as the volume fraction  $\phi$  of particles is increased. We use confocal microscopy to directly observe particle motion within dense samples with  $\phi$  ranging from 0.4 to 0.7. Our binary mixtures have a particle diameter ratio  $d_S/d_L = 1/1.3$  and particle number ratio  $N_S/N_L = 1.56$ , which are chosen to inhibit crystallization and enable long-time observations. Near the glass transition we find that particle dynamics are heterogeneous in both space and time. The most mobile particles occur in spatially localized groups. The length scales characterizing these mobile regions grow slightly as the glass transition is approached, with the largest length scales seen being  $\sim 3$  small particle diameters. The glass transition occurs at  $\phi_g \approx 0.58$ , with characteristic signs of aging observed for all samples with  $\phi > \phi_g$ .

PACS numbers: 62.43.Fs (glasses), 64.70.Pf (glass transitions), 82.70.Dd (colloids), 61.20.Ne (structure of simple liquids)

Keywords:

## I. INTRODUCTION

As the temperature of a glass-forming liquid is lowered, the viscosity rises by many orders of magnitude, becoming experimentally difficult to measure, with little change in the structure [1, 2, 3, 4]. The origin of the slowing dynamics is not clear, despite much experimental, computational, and theoretical investigations. One intriguing observation is that as a sample approaches the glass transition, the motion within the sample becomes spatially heterogeneous [5, 6]. While overall motion within the sample slows, some regions exhibit faster dynamics than the rest of the sample, and over time these mobile regions arise and disappear throughout the sample. Within the mobile region particles move cooperatively, forming spatially extended clusters and strings [7, 8, 9].

We study the glass transition of binary colloidal suspensions using confocal microscopy [10]. Because colloidal particles are large and slow enough to observe directly, suspensions are attractive systems in which to study slowing dynamics [11]. The control parameter is the particle volume fraction  $\phi$ , with increasing  $\phi$  leading from the liquid to glassy state [11, 12]. We use binary suspensions (mixtures of two particle species) to inhibit crystallization. This allows us to take data over many hours, a time scale in which a monodisperse sample would crystallize [13]. Furthermore, this lets us investigate the role the two particle species play in the dynamics; prior work has suggested that small particles play a lubricating role in the local dynamics [14].

The confocal microscope enables direct visualization of the interior of the sample, and we follow the motion of several thousand colloidal particles within each sample [10]. Particles move in spatially heterogeneous groups, and we characterize this motion using two-particle two-time correlation functions [15, 16, 17] that have previously been used on monodisperse suspensions [18]. From these we extract a length-scale for the heterogeneity, which increases as the glass transition is approached. By simultaneously tracking both large and small particles, we can observe the similarities and differences between the two species' dynamics. In particular, we see that small local composition fluctuations influence mobility. As might be expected, regions with more large particles tend to be less mobile, while those with more small particles tend to be more mobile.

## II. EXPERIMENTAL METHOD

Suspensions are prepared from poly-(methyl-methacrylate) (PMMA) colloids stabilized sterically by a thin layer of poly-12-hydroxystearic acid [11]. Mixtures are binary, with a large particle mean radius  $a_L = 1.55 \mu\text{m}$  and small particle mean radius  $a_S = 1.18 \mu\text{m}$ , the same size particles used in prior work by our group [19]. The polydispersity is 5%; each individual particle species can crystallize in a monodisperse suspension. Separately from the polydispersity, the mean particle radii each have an uncertainty of  $\pm 0.02 \mu\text{m}$ . The number ratio of small particles to large particles is  $N_S/N_L = 1.6$ , resulting in a volume fraction ratio  $\phi_S/\phi_L \approx 0.70$ . The control parameter is the total volume fraction  $\phi = \phi_S + \phi_L$ . All particles

---

\*Electronic address: takayuki.narumi@wpi-aimr.tohoku.ac.jp

are fluorescently dyed and suspended in a density- and index-matched mixture of decalin and cyclohexyl bromide to prevent sedimentation and allow us to see into the sample. Particles are slightly charged as a result of the dyeing process and this particular solvent mixture [13]. We note that crystallization and segregation were not observed to occur during the course of our measurements.

Suspensions are sealed in microscope chambers and confocal microscopy is used to observe the particle dynamics at ambient temperature [10, 20]. A representative two-dimensional image is shown in Fig. 1. A volume of  $55 \times 55 \times 20 \mu\text{m}^3$  can be taken at speeds of up to 1 Hz. (As will be shown later, in these concentrated samples, particles do not move significantly on this time scale.) To avoid influences from the walls, we focus at least  $25 \mu\text{m}$  away from the coverslip.

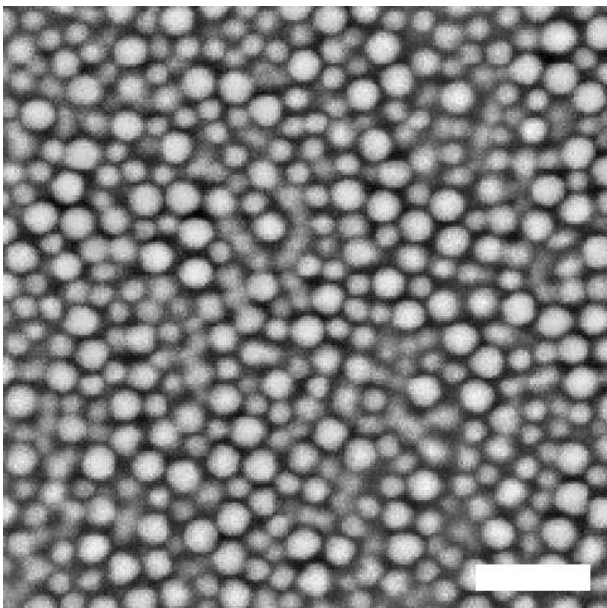


FIG. 1: A two-dimensional image of our sample taken by a confocal microscope. The size of this image is  $55 \times 55 \mu\text{m}^2$ , and the scale bar represents  $10 \mu\text{m}$ .

Within each three-dimensional image, we identify both large and small particles. In practice this is accomplished with a single convolution that identifies spherical, bright regions [21]; the convolution kernel is a three-dimensional Gaussian with a width chosen to match the size of the image of a large particle. The distribution of object sizes is typically bimodal, and the two peaks can be identified with small and large particles. This particular method is the same as is normally used to follow particle motion in two dimensions, which normally can achieve sub-pixel resolution in particle positions [21]. However, given that a single convolution kernel is used to identify both particle types, in practice when applied to our binary samples in three dimensions, we do not achieve this accuracy. In practice, our uncertainty in locating particle positions is

set by the pixel scale and is  $0.2 \mu\text{m}$  in all three dimensions. However, we do achieve accurate discrimination between large and small particles with this method, with less than 1% of the particles misidentified.

### III. RESULTS AND DISCUSSION

#### A. Structural characteristics

We begin by looking at the structure of the binary sample. Shown in Fig. 2 is the pair correlation function  $g(r)$  of a sample with volume fraction  $\phi = 0.57$ .  $g(r)$  relates to the likelihood of finding a particle a distance  $r$  away from a reference particle. The dotted line is for correlations between two small particles, with a peak at  $\approx 2a_S = 2.36 \mu\text{m}$ , confirming our small particle radius. Likewise the dashed line shows correlations between two large particles, peaking at  $\approx 2a_L = 3.10 \mu\text{m}$ . When  $g(r)$  is calculated for all particles, regardless of size, the result is the solid line in Fig. 2. A lower, slightly broader, peak is found near the average diameter of  $a_L + a_S = 2.73 \mu\text{m}$ .

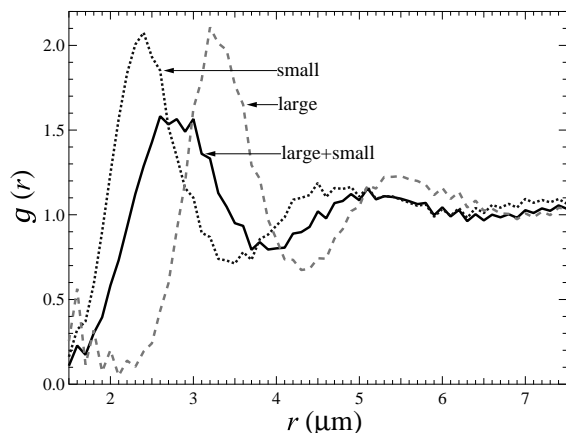


FIG. 2: The pair correlation function  $g(r)$  for a sample with volume fraction  $\phi = 0.57$ . The solid line represents  $g(r)$  for both large and small particles combined; the dashed line that of large particles alone; and the dotted line that of small particles alone.

#### B. Dynamical slowing

We first consider how the motion of particles slows as the volume fraction increases and approaches the glass transition. Figure 3 shows results of the mean square displacement (MSD)  $\langle \Delta \mathbf{r}_i^2 \rangle$  of large and small particles, where  $\Delta \mathbf{r}_i = \Delta \mathbf{r}_i(\Delta t)$  denotes the displacement of  $i$ -th particle in lag time  $\Delta t$ , and the brackets an average over all particles and times observed. Figure 3 shows that as the volume fraction increases, particle motion slows significantly, as expected. At  $\phi = 0.4$ , small particles

take tens of seconds to move a distance  $a_S^2 = 1.4 \mu\text{m}^2$ ; at  $\phi = 0.59$  the time has grown to more than  $10^4$  s. For the lowest volume fraction samples, comparing the two particle species, we find that  $\langle \Delta r_S^2 \rangle / \langle \Delta r_L^2 \rangle \approx a_L / a_S$ , as expected from the Stokes-Einstein equation.

As the volume fraction increases, the MSD plots show a characteristic plateau, interpreted as ‘‘cage trapping.’’ Particles cannot diffuse freely, but instead are surrounded by their nearest neighbor particles which form a transient cage [22, 23, 24, 25, 26, 27]. The upturn in the MSD curve is identified with the rearrangements of the cage, allowing the particle within the cage to move to a new location, perhaps caged by different particles. Although the smaller particles move faster than the large particles, MSD curves for both show upturns at similar time scales, indicating that their dynamics are strongly coupled [14].

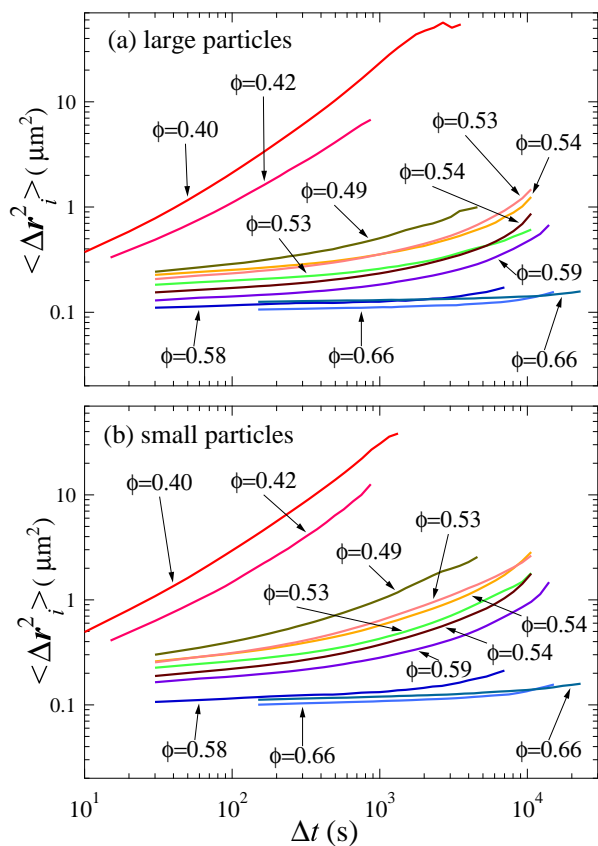


FIG. 3: (Color online) A log-log plot of mean square displacement versus time lag for large particles (a) and small particles (b). Note that our resolution means we cannot measure mean square displacement values less than  $0.1 \mu\text{m}^2$ , and thus the plateau height of curves for the highest volume fraction data is set by this limit, rather than the dynamics. The slight upturn for those curves at large values of  $\Delta t$  is above our resolution limit.

For the samples with  $\phi \geq \phi_g \approx 0.58$ , the MSD curves are nearly flat, suggesting that on our experimental time scales, these samples behave as glasses.

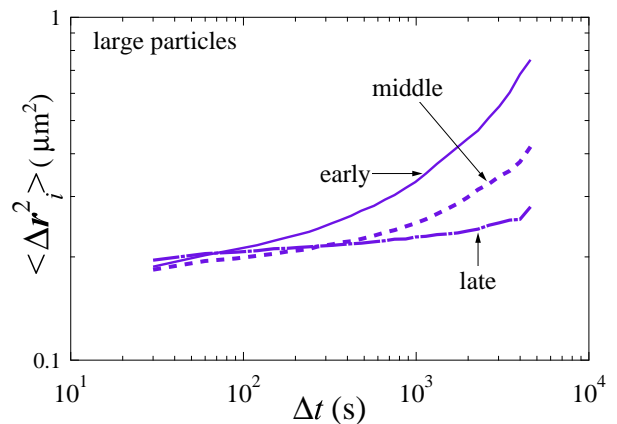


FIG. 4: (Color online) MSD plot taken of the same  $\phi = 0.59$  sample from three different times (early, middle, late). The time-dependence of  $\langle \Delta r^2 \rangle$  is clearly seen, indicating the presence of aging. As  $\phi = 0.59$  is the lowest volume fraction in which this behavior is seen, we conclude that the glass transition occurs below at  $\phi_g \approx 0.58$

Glasses are fundamentally non-equilibrium systems, so that physical properties for glasses depend on the preparation history in general and, in particular, the time since they were initially formed. This time-dependence is known as aging, and can be quantified by examining the MSD at different times since the start of the experiment [14, 28, 29]. Figure 4 shows MSD data from  $\phi = 0.59$ . The top/middle/bottom curve is data from the motion over the first/second/third of the experimental run. The sample is most active immediately after being formed, and continues to slow down as time elapses. The aging of the MSD appears in samples for  $\phi \geq 0.58$ , while no samples for  $\phi < 0.58$  show aging. From the onset of aging, we conclude that the glass transition point is at volume fraction  $\phi \approx 0.58$ , similar to that seen for monodisperse samples [11]. Note that our particle size uncertainty of  $\pm 0.02 \mu\text{m}$  (radius) leads to a systematic volume fraction uncertainty of  $\pm 4\%$ , so our estimate is  $\phi_g = 0.58 \pm 0.02$  as a comparison with prior work.

Particles involved in a cage rearrangement event move significant distances compared to when they are caged, and prior work noted that the distribution of displacements is unusually broad on the time scale of the rearrangement [25, 30]. This is quantified by calculating the non-Gaussian parameter  $\alpha_2(\Delta t)$ , which for a one-dimensional distribution of displacements is defined as

$$\alpha_2(\Delta t) = \frac{\langle \Delta x^4 \rangle}{3\langle \Delta x^2 \rangle^2} - 1, \quad (1)$$

where  $\Delta x = \Delta x(\Delta t)$  denotes the one-dimension displacement for time lag  $\Delta t$  [31]. If the distribution of displacements  $\Delta x$  is Gaussian, then  $\alpha_2 = 0$  by construction. If events with large displacements are more common than would be expected from a Gaussian distribution, then  $\alpha_2 > 0$ . Figure 5 shows the results of the

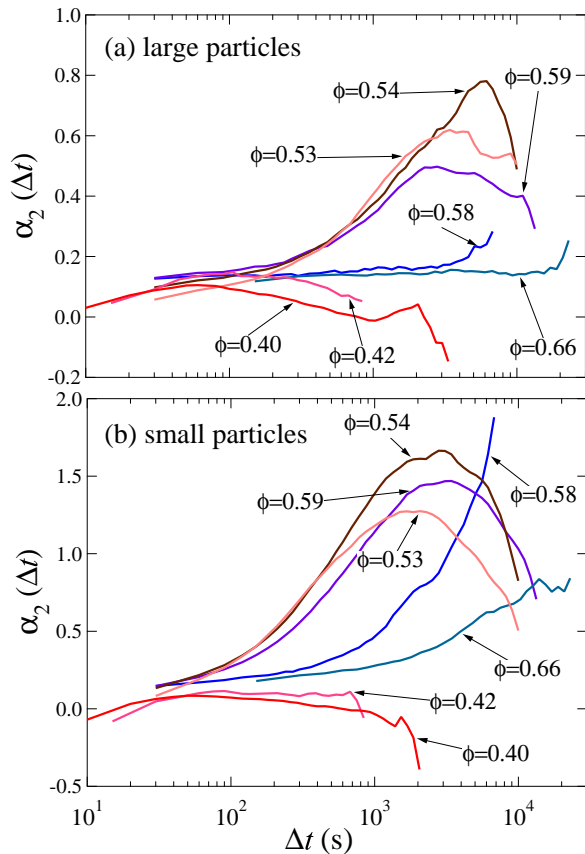


FIG. 5: (Color online) A semi-log plot of the Non-Gaussian Parameter  $\alpha_2$  versus lag time for large particles (a) and small particles (b). Since  $\alpha_2$  is sensitive to noise, we show only a few results.

non-Gaussian parameter (NGP) for one-dimension displacements of large and small particles. The curves peak at time scales where cage rearrangements are most important [7, 9], and thus coincides with the upturn of the MSD curves.  $\alpha_2$  is fairly sensitive to experimental noise, and thus we only show a few curves in Fig. 5. (For example, the downturns at large  $\Delta t$  for the low volume fraction curves are probably not real.)

Figure 5 also reveals that the motions of the small particles are more heterogeneous, with the maximum NGP peaking above 1.5 for the small species but only reaching 0.8 for the large species. This is consistent with recent observations of aging binary colloidal glasses, which likewise found the small particles had more “non-Gaussian” motion [14].

From Figs. 3 and 5 we conclude that the dynamics of the large and small particles are qualitatively the same, although with small quantitative differences. In particular, the time scale over which particles escape cages is the same for both, as is the time of peak non-Gaussianity. In much of the subsequent analysis, therefore, we consider both species together in order to obtain better statistical

validity.

### C. Local environment influences mobility

We wish to understand the origins of dynamical heterogeneity. For a hard-sphere system, or an overdamped system such as our experimental colloidal suspension, the only variable is the local structure. Clearly structure has some relation with particle mobility [32], although this relationship may be difficult to see and not directly predictive in nature [33]. Prior work found that more disordered environments are weakly correlated with higher particle mobility [25, 29], and a recent study of aging binary colloidal glasses found a relation between the local composition and the mobility [14].

We quantify a particle’s local environment by counting its nearest neighbors  $N_{NN}$ , defined as particles closer than the first minimum of the pair correlation function for the large particles,  $3.8 \mu\text{m}$  (Fig. 2), and distinguish between large and small neighbors. Figure 6 shows that the number of neighbors of a given type has a strong influence on the mobility of a particle. Particles with more large neighbors have, on average, a lower mobility, while those with more small neighbors a larger mobility. These observations agree with studies of aging in binary colloidal glasses, [14] and are reminiscent of prior rheological observations of binary suspensions [34, 35, 36] which noted that binary mixtures have lower viscosities than single-component samples with equivalent total volume fraction. The reasoning is that binary suspensions can in general be packed to higher volume fractions, and so have more free volume than monodisperse samples at the same volume fraction. Figure 6 suggests that the small particles indeed “lubricate” large particles, as previously proposed [36] Conversely, large neighbors significantly inhibit the motion of both large and small particles. The lubricant effect for large particles (which have less free volume) is less pronounced, agreeing with prior observations of monodisperse suspensions which found that regions of mobility correlated with regions of larger free volume. [25]

### D. Cooperative motions

In dense supercooled liquids, it is known that the dynamics are anomalous, with the large displacements rare, but more common than a Gaussian distribution would predict. It is also clear that, in many materials, the particles that have larger than average displacements are distributed in a spatially heterogeneous fashion [6, 7]. In monodisperse colloidal systems, direct imaging using microscopy found that particles rearrange in cooperative groups [8, 9, 37]. Following the prior work, we characterize the cooperative nature of colloidal rearrangements by studying the dynamics over a time scale  $\Delta t^*$  that corresponds to the maximum of the NGP [7, 9]. The

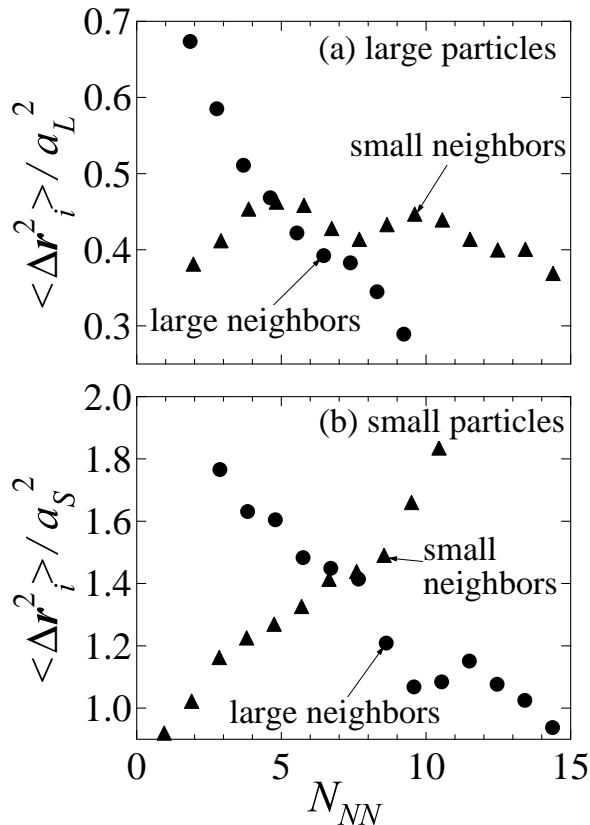


FIG. 6: Large particle mobility as a function of the number of large and small nearest neighbors  $N_{NN}$ . The panel (b) shows small particle mobility. Mobility is very sensitive to the number of large neighbors, decreasing sharply as the number of large neighbors increases. The number of smaller neighbors has a weaker, yet measurable, impact. These data are for volume fraction  $\phi = 0.53$ , using a time scale  $\Delta t = 3780$  s to define displacements.

maximum displacement of a particle over that time  $D_i$  is defined as

$$D_i(t) := \max_{t, t+\Delta t^*} (|\mathbf{r}_i(t_2) - \mathbf{r}_i(t_1)|) \quad (2)$$

where  $\max_{t, t+\Delta t^*}(X)$  is the maximum value of  $X$  using times  $t_1, t_2$  such that  $t \leq t_1 < t_2 \leq t + \Delta t^*$ . Taking the maximum displacement results in a quantity that is less sensitive to random Brownian motion than the ordinary displacement  $\Delta r$ . Following prior work, [7, 9] a threshold  $D^*(\phi)$  is chosen such that on average, 5% of the particles at any given time have  $D_i(t) > D^*$ . These particles are termed “mobile particles” and generally are the ones undergoing cage rearrangements. (Note that at any particular time, the fraction of particles matching this definition is not required to be 5% [20]).

Figure 7 shows snapshots of our system, highlighting the mobile particles. Clusters of these mobile particles are visible, in agreement with previous work which

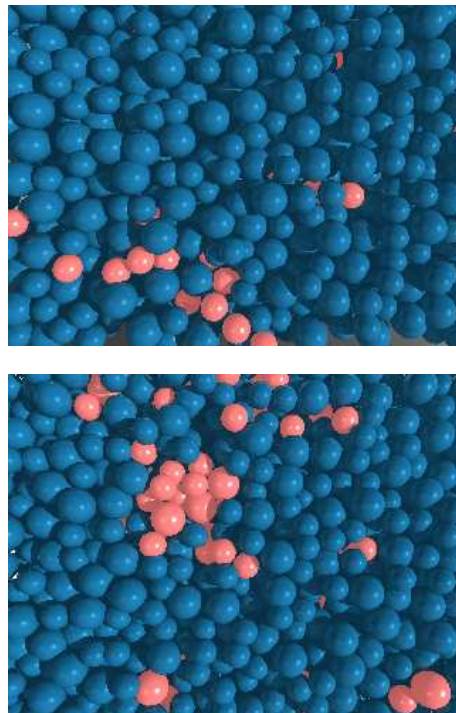


FIG. 7: (Color online) Snapshots of system for  $\phi = 0.53$  (upper) and  $\phi = 0.59$  (bottom). The red particles are mobile, all other particles are blue. Mobile particles are defined as those making the largest displacements at this particular moment in time; see text for further details. We set the time lag for the displacement as the cage breaking time scale (the peak time of the NGP  $t_{NGP}$ ) which is  $\Delta t^* = 3000$  s for  $\phi = 0.53$  and  $t^* = 5070$  s for  $\phi = 0.59$ .

found similar mobile regions [7, 9, 14]. The clusters are somewhat smaller than those seen previously in single-component colloidal suspension [9]; apparently the dynamics in binary mixtures are less spatially heterogeneous. Our result is in agreement with the results of a simulation study for polydisperse hard-disk systems [38], which found that polydispersity reduces dynamic heterogeneity. It is also apparent in Fig. 7 that the number of mobile particles is similar for the two particle sizes. This reinforces our earlier decision to consider both large and small particles as one for statistical calculations.

### E. Correlation functions and dynamic length scales

Pictures such as Fig. 7 are qualitative evidence of dynamical heterogeneity. For quantitative information, we consider the vector and scalar spatial-temporal correlation functions [17]  $S_{\Delta r}(R, \Delta t)$  and  $S_{\delta r}(R, \Delta t)$  defined as

$$S_{\Delta r}(R, \Delta t) := \frac{\langle \Delta \mathbf{r}_i \cdot \Delta \mathbf{r}_j \rangle_{\text{pair}}}{\langle \Delta r^2 \rangle} \quad (3)$$

$$S_{\delta r}(R, \Delta t) := \frac{\langle \delta r_i \delta r_j \rangle_{\text{pair}}}{\langle (\delta r)^2 \rangle}. \quad (4)$$

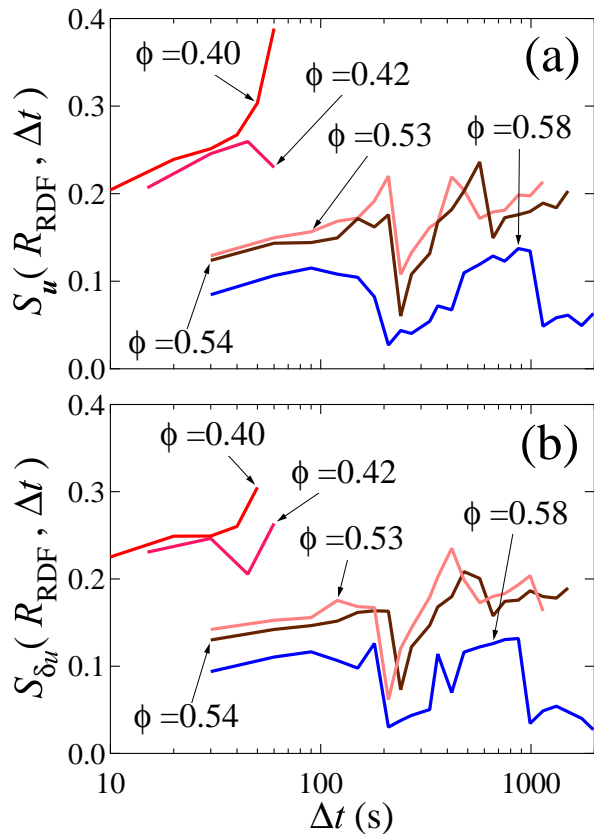


FIG. 8: (Color online) Semi-log plot of the correlation functions in which the distance  $R = 2.73 \mu\text{m}$  is set as the first peak of the pair correlation function for all (large+small) particles. (a) represents the vector correlation (Eqn. (3)), and (b) the scalar correlation (Eqn. (4)).

The vector function  $S_{\Delta\mathbf{r}}(R, \Delta t)$  characterizes correlations in the vector displacements  $\Delta\mathbf{r}_i = \mathbf{r}_i(t + \Delta t) - \mathbf{r}_i(t)$ ; the corresponding scalar function  $S_{\delta r}(R, \Delta t)$  uses the scalar distance  $\delta r_i = |\Delta\mathbf{r}_i| - \langle |\Delta\mathbf{r}_i| \rangle$ . The angle brackets  $\langle \rangle$  denote an average over all particle pairs with separation  $R$  at initial time  $t$  as well as an average over  $t$ . The denominators of both correlation functions are averaged over all particles and time, and do not depend on  $R$ . The correlation function defined by Eqn. (3) indicates a vector correlation, and that defined by Eqn. (4) a scalar correlation. If particles correlate perfectly, the both correlation functions are unity. These correlation functions give information about spatial correlations for fixed lag time  $\Delta t$ , and about temporal dependence of the correlations for fixed separation  $R$ . We calculate these functions for all pairs of particles, without concern for the particle sizes, both to improve our statistics and because we do not find significant differences for large and small particles only.

Figure 8 shows the lag time dependence of these correlation functions, in which the distance  $R$  is set as the

first peak distance of the pair correlation function  $g(r)$  (see Fig. 2). At time scales larger than those shown in Fig. 8, the results become too uncertain, due to lack of data. In intermediate volume fraction region ( $\phi < 0.6$ ), both correlation functions increase with  $\Delta t$ . In conjunction with Fig. 3, this suggests that larger motions are more correlated with the motions of their neighboring particles. In particular, as  $\Delta t \rightarrow t_{\text{NGP}}$ , the scalar correlation is clearly important and thus cooperative motions are relevant for the relaxation. This agrees with prior experiments [9, 18].

For glassy samples ( $\phi > 0.6$ ) the correlation functions show no real dependence on the lag time. Additionally, their values are small, suggesting that there is little correlation of the motion of neighbors. This is both because there is little overall motion in glassy samples (see Fig. 3) and also the motion that does occur is dominated by Brownian motion within the cage, which is less correlated than the motions responsible for cage rearrangements [25].

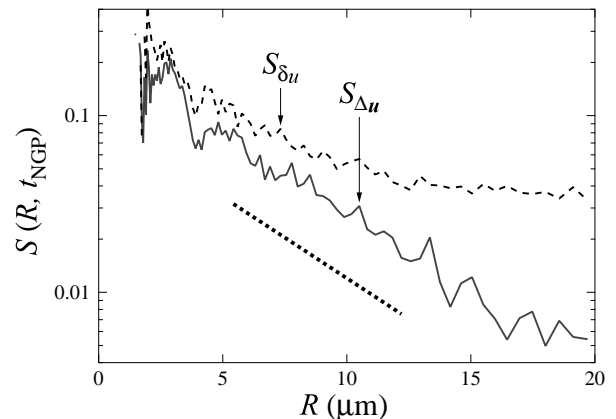


FIG. 9: Semi-log plot of the spatial correlation functions of  $\phi = 0.54$ , where the time lag is set as  $\Delta t_{\text{NGP}} = 3030\text{s}$ . The dotted line represents an exponential function.

To consider the spatial dynamical heterogeneities, we plot the correlation functions as a function of  $R$  in Fig. 9 (for  $\phi = 0.54$ ; results for other volume fractions are similar). For small separations around  $R = 3.5 \mu\text{m}$ , there is a dip in the correlation functions, which corresponds to the dip in the pair correlation function at the same position (Fig. 2); the peak around  $R = 2.8 \mu\text{m}$  likewise corresponds to the peak of the pair correlation function. Thus, a particle's motion is correlated with that of its nearest neighbors, while particles separated by a less structurally favorable distance are less likely to have correlated motion.

We fit our data with an exponential function  $S \simeq A \exp(-R/\xi)$  and extract the decay length  $\xi$ . Figure 10 shows both the vector (circles) and scalar (squares) decay lengths vs. volume fraction. Both length scales gradually increase as the volume fractions increase, although the increase is more pronounced for the scalar length. These

lengths do not appear to diverge as the glass transition ( $\phi_g \approx 0.58$ ) is approached, consistent with simulations of binary Lennard-Jones mixtures [39]. The largest length scale seen is  $\approx 7 \mu\text{m} \approx 6a_S \approx 4.5a_L$ , similar to prior studies of monodisperse colloids [18].

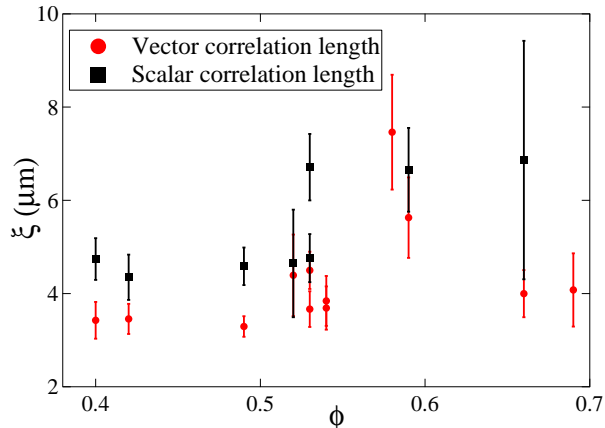


FIG. 10: (Color online) The relationship between the length scales and the volume fraction. The symbols indicate the average value, and the error bars show the range of values found for different lag times  $\Delta t$ . These length scales are extracted from the vector correlation function for all particles (large + small). For volume fractions where points are missing, the scalar mobility correlation function did not decay exponentially and thus no length scale was determined.

#### IV. SUMMARY

We have used confocal microscopy to study three-dimensional motion of particles in binary colloidal mix-

ture. The volume fraction  $\phi$  is varied from 0.4-0.7 and a glass transition, characterized by aging dynamics, is found at  $\phi \approx 0.58$ . The dynamics of large and small particles are qualitatively similar. At volume fractions approaching the glass transition, both show an increase in motion at the same characteristic cage breaking time scale. This time scale also corresponds with the time over which the motion of both particles have the least Gaussian distribution. The number of mobile particle of large and small particle is also comparable. Particle motion is facilitated by the presence of small neighbors, and inhibited by large neighbors, consistent with the idea that small particles serve as lubricants. We have investigated the vector and scalar correlation functions and extracted specific length scales associated with the decay in correlation. This length slightly increases with volume fraction, although it does not appear to diverge as the glass transition is approached.

#### Acknowledgments

We thank the Soft Condensed Matter Group of the Physics Department in Emory University for fruitful discussions, in particular J. M. Lynch and G. C. Cianci. T. N. was supported by the 21st Century COE Program “International COE of Flow Dynamics” of Tohoku University. S.V.F. and E. R. W. were supported by the National Science Foundation under Grant No. DMR-0239109, and E. R. W. was additionally supported by the NSF under Grant No. CHE-0910707. We thank A. Schofield and W. C. K. Poon for providing our colloidal samples.

- 
- [1] C. A. Angell, *Science* **267**, 1924 (1995).
  - [2] F. H. Stillinger, *Science* **267**, 1935 (1995).
  - [3] M. D. Ediger, C. A. Angell, and S. R. Nagel, *J. Phys. Chem.* **100**, 13200 (1996).
  - [4] C. A. Angell, K. L. Ngai, G. B. McKenna, P. F. McMillan, and S. W. Martin, *J. App. Phys.* **88**, 3113 (2000).
  - [5] G. Adam and J. H. Gibbs, *J. Chem. Phys.* **43**, 139 (1965).
  - [6] M. D. Ediger, *Annu. Rev. Phys. Chem.* **51**, 99 (2000).
  - [7] C. Donati, J. F. Douglas, W. Kob, S. J. Plimpton, P. H. Poole, and S. C. Glotzer, *Phys. Rev. Lett.* **80**, 2338 (1998).
  - [8] W. K. Kegel and A. van Blaaderen, *Science* **287**, 290 (2000).
  - [9] E. R. Weeks, J. C. Crocker, A. C. Levitt, A. Schofield, and D. A. Weitz, *Science* **287**, 627 (2000).
  - [10] V. Prasad, D. Semwogerere, and E. R. Weeks, *J. Phys.: Cond. Matt.* **19**, 113102+ (2007).
  - [11] P. N. Pusey and W. van Meegen, *Nature* **320**, 340 (1986).
  - [12] W. van Meegen and P. N. Pusey, *Phys. Rev. A* **43**, 5429 (1991).
  - [13] U. Gasser, E. R. Weeks, A. Schofield, P. N. Pusey, and D. A. Weitz, *Science* **292**, 258 (2001).
  - [14] J. M. Lynch, G. C. Cianci, and E. R. Weeks, *Phys. Rev. E* **78**, 031410 (2008).
  - [15] P. H. Poole, C. Donati, and S. C. Glotzer, *Physica A: Statistical and Theoretical Physics* **261**, 51 (1998).
  - [16] C. Donati, S. C. Glotzer, and P. H. Poole, *Phys. Rev. Lett.* **82**, 5064 (1999).
  - [17] B. Doliwa and A. Heuer, *Phys. Rev. E* **61**, 6898 (2000).
  - [18] E. R. Weeks, J. C. Crocker, and D. A. Weitz, *J. Phys.: Cond. Matt.* **19**, 205131 (2007).
  - [19] C. R. Nugent, K. V. Edmond, H. N. Patel, and E. R. Weeks, *Phys. Rev. Lett.* **99**, 025702 (2007).
  - [20] A. D. Dinsmore, E. R. Weeks, V. Prasad, A. C. Levitt, and D. A. Weitz, *App. Optics* **40**, 4152 (2001).
  - [21] J. C. Crocker and D. G. Grier, *J. Colloid Interf. Sci.* **179**, 298 (1996).
  - [22] E. Rabani, D. J. Gezelter, and B. J. Berne, *J. Chem.*

- Phys. **107**, 6867 (1997).
- [23] B. Doliwa and A. Heuer, Phys. Rev. Lett. **80**, 4915 (1998).
- [24] A. Kasper, E. Bartsch, and H. Sillescu, Langmuir **14**, 5004 (1998).
- [25] E. R. Weeks and D. A. Weitz, Phys. Rev. Lett. **89**, 095704 (2002).
- [26] E. R. Weeks and D. A. Weitz, Chem. Phys. **284**, 361 (2002).
- [27] P. M. Reis, R. A. Ingale, and M. D. Shattuck, Phys. Rev. Lett. **98** (2007).
- [28] R. E. Courtland and E. R. Weeks, J. Phys.: Cond. Matt. **15**, S359 (2003).
- [29] G. C. Cianci, R. E. Courtland, and E. R. Weeks, Solid State Comm. **139**, 599 (2006).
- [30] W. Kob, C. Donati, S. J. Plimpton, P. H. Poole, and S. C. Glotzer, Phys. Rev. Lett. **79**, 2827 (1997).
- [31] A. Rahman, Phys. Rev. **136**, A405 (1964).
- [32] A. Widmer-Cooper, P. Harrowell, and H. Fynewever, Phys. Rev. Lett. **93**, 135701 (2004).
- [33] J. C. Conrad, F. W. Starr, and D. A. Weitz, J. Phys. Chem. B **109**, 21235 (2005).
- [34] R. L. Hoffman, J. Rheology **36**, 947 (1992).
- [35] P. D'Haene and J. Mewis, Rheologica Acta **33**, 165 (1994).
- [36] S. R. Williams and W. van Meegen, Phys. Rev. E **64**, 041502+ (2001).
- [37] A. H. Marcus, J. Schofield, and S. A. Rice, Phys. Rev. E **60**, 5725 (1999).
- [38] T. Kawasaki, T. Araki, and H. Tanaka, Phys. Rev. Lett. **99**, 215701 (2007).
- [39] T. Narumi and M. Tokuyama, Phil. Mag. **88**, 4169 (2008).